Article

Not peer-reviewed version

A New Rotary Magnetorheological Damper for a Semi-Active Suspension System of low-Floor Vehicles

Yu-Jin Park , Byung-Hyuk Kang , Seung-Bok Choi *

Posted Date: 19 March 2024

doi: 10.20944/preprints202403.1103.v1

Keywords: Magnetorheological Fluid; Rotary MR damper; Low-Floor Vehicles; Finite Element Analysis; Magnetic Analysis; Response Time; Damping Force

Article

A New Rotary Magnetorheological Damper for a Semi-Active Suspension System of Low-Floor Vehicles

Yu-Jin Park [1], Byung-Hyuk Kang [2] and Seung-Bok Choi [3,4,*]

[1] Korea Initiative for fostering University of Research & Innovation, Inha University, Incheon 21999, Republic of Korea; eugene5059@inha.ac.kr
[2] Department of Mechanical Engineering, The State University of New York, Korea (SUNY Korea), Incheon 21985, Republic of Korea; 1357op@gmail.com
[3] Department of Mechanical Engineering, The State University of New York, Korea (SUNY Korea), Incheon 21985, Republic of Korea; seungbok.choi@sunykorea.ac.kr
[4] Department of Mechanical Engineering, Industrial University of Ho Chi Minh City (IUH), Ho Chi Minh City 70000, Vietnam
* Correspondence: seungbok.choi@sunykorea.ac.kr

Abstract: This study explores the significance of active suspension systems for vehicles with lower chassis compared to conventional ones, aiming at the development of future automobiles. Conventional linear MR (Magneto-Rheological) dampers were found inadequate in ensuring sufficient vibration control because the vehicle's chassis becomes lowered in the unmanned vehicles or purposed based vehicles. As an alternative, a rotary type of MR damper is proposed in this work. The proposed damper is designed based on pre-specified design parameters through mathematical modeling and magnetic field analyses. Subsequently, a prototype of the rotary MR damper identical to the design is fabricated, and effectiveness is shown through experimental investigations. In configuring the experiments, a proportional-integral (PI) controller is employed for current control to reduce the response time of the damper. The results presented in this work provides useful guidelines to develop a new type of MR damper applicable to various types of future vehicles' suspension systems with low distance from the tire to the body floor.

Keywords: magnetorheological fluid; rotary MR damper; low-floor vehicles; finite element analysis; magnetic analysis; response time; damping force

1. Introduction

It is well known that vehicle suspension systems can be classified into the passive, the semi-active, and active types. Recently, many studies have been conducted about the semi-active suspension system due to its enhanced ride comfort and road holding with the fail-safe capability compared to the other two types. Especially, since the magnetorheological (MR) fluid has been applied to several types of dynamic systems to control unwanted vibrations, more attention and research on the semi-active suspension of the vehicles. These numerous works could bring both MR fluid itself and MR damper for the vehicle suspension system to the corresponding market as commercial outcomes [1,2]. In fact, there are many types of MR dampers applicable the vehicle suspension systems: mono-tube type with and without the bypass hole, twin-tube type with the single-end, mono-tube type with double-end, mono-tube type with the external magnetic circuit core and pinch node type [3–6]. Each type has advantages and disadvantages over the other types. For example, the mono-tube with the single-ended MR damper produces the maximum damping force at same conditions, while the mono-tube type with the external core MR damper has the largest stroke motion during the driving operation. However, most of MR dampers proposed or developed for the vehicle suspension systems so far are the linear types to provide the translation stroke in the direction of up and down. This large stroke motion in vertical direction is possible since the space (or height)

 doi:10.20944/preprints202403.1103.v1

from the wheel to the floor of the car body is sufficient (around ±30mm) for the installation of the linear MR damper vertically. Figure 1 shows a schematic configuration of the typical linear MR damper which consists of MR piston assembly, gas chambers and magnetic circuits cores.

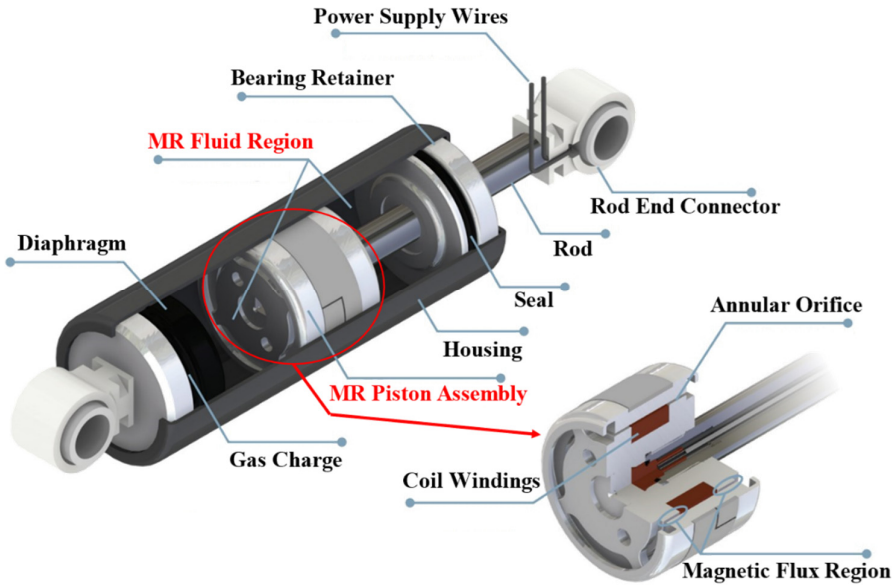

Figure 1. Schematic configuration of the linear MR damper.

As for the research of the rotary MR dampers, Giorgetti et al. [7] firstly introduced a rotary MR damper applicable to the front-wheel suspension of a compact car. Some advantages of the proposed rotary MR damper such as the small quantity of fluid and the low abrasion of the seals were discussed, follows by a swinging type of the rotary MR damper was designed to reduce the space requirement and mechanical resistance on the heavy off-road profiles. After analyzing the flow motion of the annular duct, several principal design parameters were determined. The operational angle is chosen by 60deg to reproduce all the movements of the previous suspension motion. It has been shown from measurement that the damping torque of the rotary MR damper can cover the damping range of the conventional linear MR damper. It is noted here that the verification of the results presented in this work is not possible since the information of many design parameters and magnetic analysis is not presented. Lee et al. [8] designed a rotary MR damper for unmanned vehicle suspension system and evaluated the field-dependent torque performance through the finite element method and experimental test. The damping torque at the disk rotating speed of 10 m/s was obtained by 239.2 and 576.78 N.m at the current 0.5 A and 1.5 A, respectively. However, in this work, the limit of the rotational angle and the height of the MR damper did not consider for the design. Thus, the operating principle of the MR damper studied in this work is the same as MR clutch in which the torque is the resistance of the servo motor to overcome a reduction in motor speed due to the increment of apparent viscosity of MR damper with respect to the current applied to. Imaduddin et al. [9] published a review article on the rotary MR damper emphasizing on the design and modeling methods. It has been mentioned that despite successful implementation of the linear MR dampers to the semi-active suspension systems of variable vehicles, there are still limitations to be resolved. For examples, the linear MR damper needs a large space to install (especially height), the inability to accommodate high wheel travel due to the risk of the buckle in the damper, a large amount of MR fluid and the less resistance to damage from foreign objects. Two types of the rotary MR damper with continuous angle and limited angle were also discussed. The configuration of the continuous type is the same as the disk-type of MR clutch and MR brake which has a relatively large design to achieve high damping torque. The limited angle type is operated by vane with the inner magnetic coil valve and the rotational angle is determined by the movement of the rotating hub connected to the vane.

 doi:10.20944/preprints202403.1103.v1

The vane type of the rotary MR damper has several benefits including the low height, compact side without any chamber, small amount of MR fluid, combination of the flow and shear mode generation by the rotational angle. However, a lot of challenging effort is still required for successful realization in practice. For example, the optimal design of the non-cylindrical shape of vane is one of the most serious problems to be resolved. Imaduddin et al. [10] also proposed a bypass rotary MR damper for the semi-active suspension system of conventional vehicles. In this design, the rotational angle was limited by 70 degree and the vane size was fixed by 40x40 mm with the radius of the vane center of 4.5 mm. The outer diameter of the rotary MR damper was determined by 50 mm to locate three magnetic cores at the center line. From the simulation, the proposed rotary MR damper produced more than 1000 N.m with 1 A and 1. 5 rad/s. It should be noted that these results were obtained without any magnetic analysis and operating angle condition.

Sapinski [11] investigated an energy harvesting system utilizing a rotary motion obtained from three components: a rotary MR damper to vary the damping characteristics, a rotary power generator producing electrical power and a conditioning electronics unit to interface with the damper and generator. This work is similar to the self-powered linear MR damper using the energy harvesting system, in which the linear MR damper is replaced by the rotary MR damper with the rotary generator. In this work, a multi-disk type of the rotary MR damper is made and connected with the generation. It has been shown that the energy recovered by the generator is sufficient to operate the rotary MR damper, but the conditioning electronics unit needs to be changed so that the harvested voltage is less than the maximum limit. Yu et al. [12] proposed a rotary MR damper consisting of two driven disks and an active rotary disk to achieve the output with a large stiffness change. In the performance evaluation via experimental test, the effects of the current, angle and frequency on the torque-angle loops and torque-frequency loops are considered. The height and width of the MR damper were chosen by 57.6 mm and 87 mm, respectively. It has been shown that the torque is increased as the angle increases, and the dynamic range is increased as the current increases, as expected. It was also observed from experimental results that the maximum torque was identified by 10 N.m. Such a low level of torque is much less than the torque of traditional linear MR damper and hence the proposed rotary MR damper does not provide any practical feasibility. It is noted here that expect the rotary MR damper, the rotational motion devices utilizing MR fluid have been worked a lot focusing on the brake, clutch, bearing and shaft vibration control [13–17].

Recently, diverse configurations of future vehicles are introduced in several places such as CES 2024 [http://www.ces.tech; [18]], held in January of this year at Las Vegas. In this technology show, several cars and concept cars have been introduced by car makers and electronics companies. It is very interesting to see that most of future cars for the unmanned mobility city (UMC) or purposed based vehicle (PBV) for a special mission have very low distance (height) from the wheel to the floor of the vehicle body. Therefore, commercially available linear MR damper cannot be installed to the limited space. Figure 2 shows the height between the wheel and the body floor of the car for the conventional and future vehicle, respectively. The photo shown in Figure 2b of the future vehicle is one of PBVs presented at CES 2024. It is clearly seen that there is a limited space to install MR damper in the vertical direction. Therefore, a new type of rotary MR damper which is applicable to the low-floor vehicle suspension systems is required.

 doi:10.20944/preprints202403.1103.v1

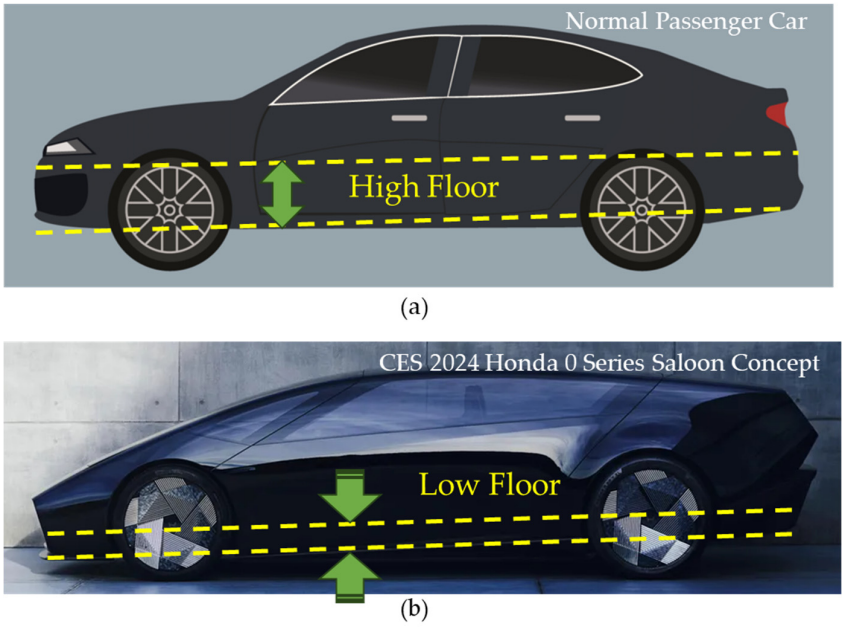

Figure 2. Height from the tire to the body floor; (a) conventional vehicle, (b) future car.

The amount of the research on the rotary MR damper for the vehicle suspension system is much less than conventional linear MR damper. It is identified from the above literature survey on the rotary MR damper, there is no study to meet the prescribed targets of design parameters and damping forces. Most of rotary MR dampers have been designed without the specified target performances. Consequently, the main technical contribution of this work is to design and manufacture the prototype of the rotary MR damper and demonstrate its effectiveness to the possibility of practical application for the future vehicles featured by very low-floor height. In this work, the vane-type of the rotary MR damper is designed to resolve the strict space limitation. The flow motion of MR fluid is then limited by the rotational angle range of the vane where both flow mode and shear mode are occurred. After analyzing the governing equations and magnetic flux distribution, principal design parameters to achieve the prescribed targets are determined. The size and number of the magnetic circuit cores are determined through the magnetic flux density of the MR damper associated with design parameters. Then, a protype is manufactured and tested to achieve the field-dependent damping force. It is noted here that the design method and results presented in this work will be useful guideline to make an efficient rotary MR damper for specialized vehicles to be appeared in UMC.

2. Configuration and Modeling

As mentioned in Introduction, in this work, desired targets (or specifications) are firstly set up to design a rotary MR damper. Since the proposed MR damper is to be installed a small-sized future car, the desired specifications are chosen as follows: (i) Maximum damping torque target: 600Nm @ 30m/s or higher, (ii) Response time for current control: within 50ms @ 90% rise time criterion, (iii) Operating angle range by the vane: +- 30 degree, (iv) maximum diameter: 150mm, (v) Maximum width: 190mm. In order to meet these targets, several configurations of the rotary MR damper are firstly investigated and created. Figure 3 presents two different types of the rotary MR damper. The first configuration depicted in Figure 3a is designed to generate damping torque by inducing rotational motion on the upper arm, thereby facilitating the flow of the MR fluid. This configuration offers the advantage of relatively straightforward construction and a wide range of rotational motion capabilities. However, it necessitates careful attention to detail in the design of the oil packing to prevent potential oil leakage between the MR damper and the cylinder contact. Moreover, the

 doi:10.20944/preprints202403.1103.v1

inclusion of a bearing guide with a sloped surface is essential for its operation. Moreover, the manufacturing process for this configuration is complex. On the other hand, the second damper structure shown in Figure 3b offers distinct characteristics and potential advantages. The flow motion of MR fluid through the orifice is easily occurred by the rotor and convenient to make as a compact size. In addition, the intensity of the magnetic field can easily control the resistance of fluid flow and hence the field-dependent damping force. Therefore, in this work, the configuration shown in Figure 3b is chosen and modified to achieve the specified targets.

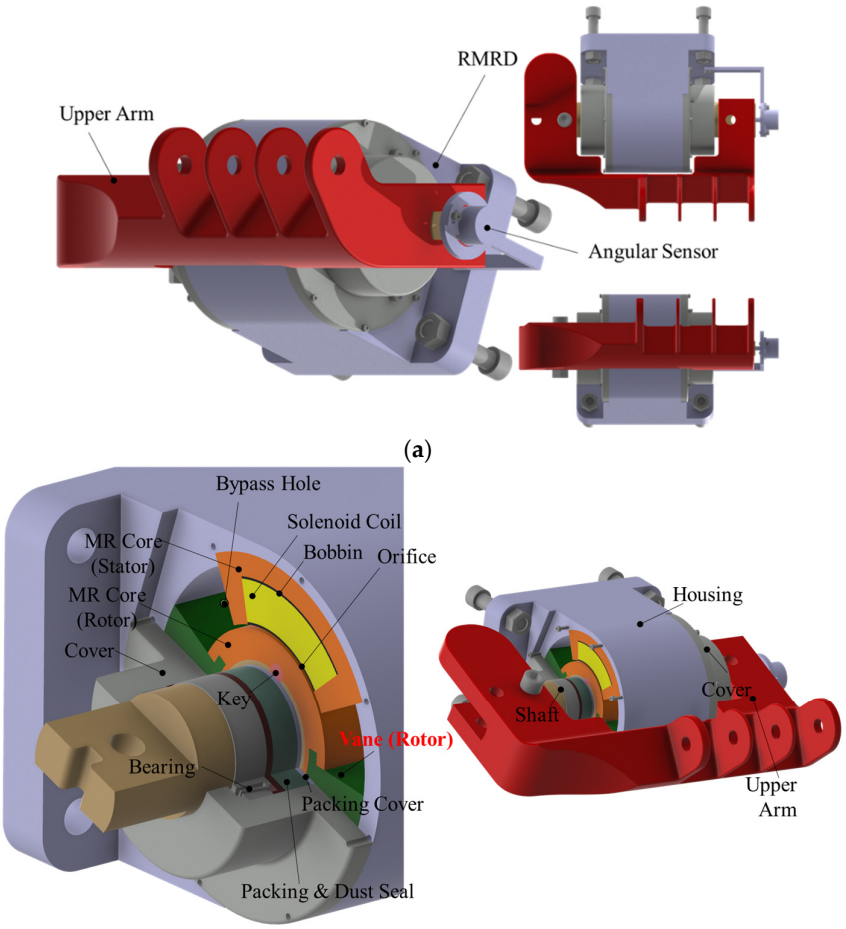

Figure 3. Configurations of the rotary MR damper: (a) cylinder type, (b) key-home type.

In this work, the configuration shown in Figure 3b is modified a little by adding the bypass holes to reduce the damping coefficient in the low frequency (low rotational speed) to acquire a good ride comfort from the starting. The modified configuration is depicted in Figure 4. This figure is useful to drive the pressure drops proportional to rotational speed and pressure drop proportional to input current. The pressure drop due to the viscosity of MR fluid and the pressure drop due to the yield stress of MR fluid is given by Equations (1) and (2) [19,20].

 doi:10.20944/preprints202403.1103.v1

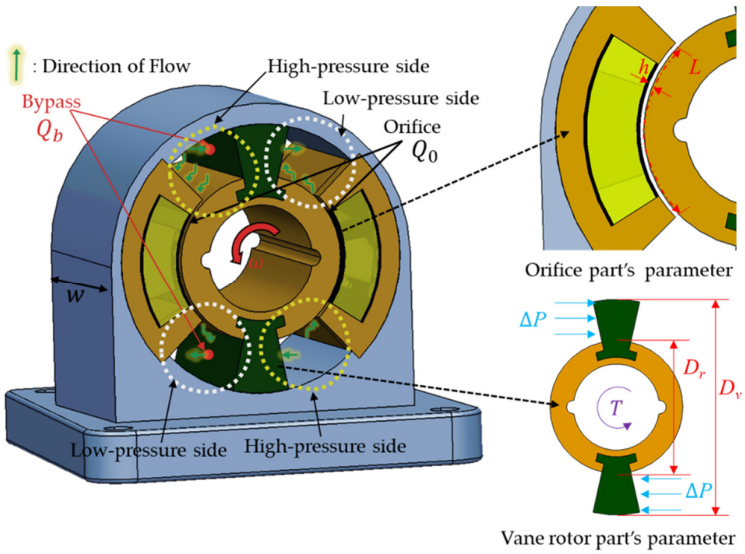

Figure 4. The schematic for flow direction and pressure drop of the rotary MR damper.

$$P_{vis} = \frac{12\eta L}{wh^2}\left(\frac{1}{h} - \frac{2D_r}{D_v^2 - D_r^2}\right) \cdot Q$$
$$Q = \frac{D_v^2 - D_r^2}{8} w \cdot \omega \quad (1)$$

$$P_y = c\frac{L_p}{h}\left|\tau_y(H)\right| \cdot sgn(\omega)$$
$$c = 2.07 + \frac{12\eta|Q|}{12\eta|Q| + 0.4wh^2\left|\tau_y(H)\right|} \quad (2)$$

$$\Delta P = P_{vis} + P_y \quad (3)$$

$$T = \frac{D_v^2 - D_r^2}{4} w \cdot \Delta P \quad (4)$$

In the above equations, Q is the total flow, ΔP is the total pressure drop, η stands for the viscosity coefficient of the MR fluid, L represents the length inside the core, w indicates the total height of the damper, D_r denotes the outer diameter of the MR core, and D_v represents the outer diameter of the vane rotor. H denotes the magnetic field intensity, ω symbolizes the angular velocity, and T refers to the static torque and $sgn(\omega)$ represents the signum function with respect the angular speed. It is identified that the pressure drop proportional to rotational speed is derived in Equation (1) and the flow rate Q is expressed similarly to Equation (1) as it occurs between the rotor and housing. The field-dependent pressure drop is dependent the yield stress of MR fluid which is a function of the current as shown in Equation (2), and $c \approx 2.07 + 1/(1 + 0.4\mathcal{I})$ bounded to the interval [2.07,3.07] [21]. The total pressure drop can be expressed as the sum of pressure drop proportional to rotational speed and pressure drop proportional to input current, as shown in Equation (3). Pseudo-static rotational force represents the static force or moment exerted on the rotating object. By utilizing the total pressure drop obtained earlier, the pseudo-static rotational force can be expressed in terms of torque as given Equation (4). Since the proposed rotary MR damper has the bypass hole, the flow direction inside the damper is indicated by the green line in Figure 4. Under the assumption of neglecting frictional forces, the total flow can be considered as the sum of the flow through the orifice and the flow through the bypass.

$$Q = Q_0 + Q_b \quad (5)$$

 doi:10.20944/preprints202403.1103.v1

However, it can be assumed that the pressure drops inside are all proportional, thus the pressure drop can be represented by Equation (6). Now, Equations (7) and (8) are derived respectively for the pressure drop relationships of the orifice and the bypass hole. Equation (8) is obtained using the Hagen-Poiseuille equation, which is a common formula used to calculate pressure drop caused by fluid flow inside a pipe. However, difficulties could be arisen in calculating the pressure drops due to the ambiguity in determining the flow rates. In this work, in order to resolve this, the pressure drop analysis is carried out using dimensionless analysis (nondimensionalization).

$$\Delta P = \Delta P_0 = \Delta P_b \tag{6}$$

$$\Delta P_0 = \frac{12\eta L}{wh^2}\left(\frac{1}{h} - \frac{2D_r}{D_v^2 - D_r^2}\right)\cdot Q_0 + c\frac{L_p}{h}\left|\tau_y(H)\right|\cdot sgn(\omega)$$

$$where\ c = 2.07 + \frac{12\eta|Q_0|}{12\eta|Q_0| + 0.4wh^2\left|\tau_y(H)\right|} \tag{7}$$

$$\Delta P_{bypass} = \frac{128\eta L_b}{\pi D_b^4 N_b}\cdot(Q - Q_0) \tag{8}$$

Figure 5 depicts a schematic of fluid flow within the parallel-plate utilized for deriving dimensionless flow rates [21]. In the above, τ_y is yield stress, h_1 is region II's height, h_2 is region I's height, D_0 is gap total (orifice), L_p is Magnetic pole length of orifice hole, D_b is gab of bypass, N_b is number of bypass hole, L_b is Magnetic pole length of bypass hole. It shows the flow for both the orifice and bypass individually, with the nomenclature for each location within the plate provided on the right. The dimensionless flow rate for the damper orifice is initially derived. Here, the key dimensionless variables, $Q^*, T^*, L^*, and\ V^*$ represent flow rate, static torque, length, and fluid velocity, respectively. They are to be utilized significantly, and the expression can sufficiently represent Equation (5). Having derived Equation (9), the relationship for the bypass can be deduced from the equations governing the bypass flow rate and pressure drop. Thus, the following equations are obtained.

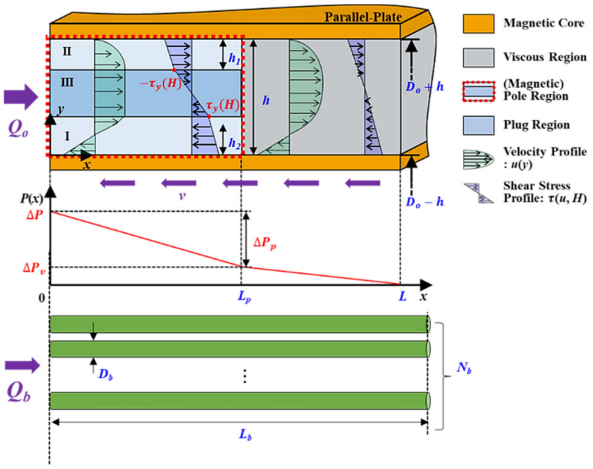

Figure 5. Non-dimensional flow rate of the rotary MR damper using the parallel-plate.

$$Q^* = 1 - \frac{3L^*V^*}{1-(0.4-L^*)T^*} - \frac{(1.4+L^*)T^*}{1+(0.4+L^*)T^*}$$

$$Q^* = \frac{12\eta LQ_0}{wh^3\Delta P},\ V^* = \frac{2\eta Lv}{h^2\Delta P},\ T^* = \frac{2L_P|\tau_y|}{h\Delta P},\ L^* = \frac{L_P}{L} \tag{9}$$

$$0 < Q^* < 1,\ \ 0 < T^* < 1,\ \ 0 < L^* < 1,$$

 doi:10.20944/preprints202403.1103.v1

$$0 < V^* < \frac{(1-(1-L^*)Q^*-T^*)^2}{L^*(1-(1-L^*)Q^*)}$$

Now, using Equation (5), the proportional relationship between the orifice and bypass leads to the derivation of equations governing the flow rate and pressure drop. The derived equation is presented by Equation (10). In this equation, a_1 represents the flow rate expression for the bypass, and a_2 denotes the relationship associated with the bypass.

$$a_1\frac{Q}{\Delta P} = \frac{a_1}{a_2} + Q^* = 1 + \frac{a_1}{a_2} - \frac{3L^*V^*}{1-(0.4-L^*)T^*} - \frac{(1.4+L^*)T^*}{1+(0.4+L^*)T^*}$$

$$a_1 = \frac{12\eta L}{wh^3},\ a_2 = \frac{128\eta L_b}{piD_b^4 N_b} \tag{10}$$

Therefore, summarizing the dimensionless pressure drop relationship is given by the following equation.

$$P^* = \frac{a_2}{a_1+a_2}\left(1 + \frac{3L^*V^{*+}P^*/6}{P^*-(0.4-L^*)T^*} + \frac{(1.4+L^*)L^*T^{*+}P^*}{P+(0.4+L^*)L^*T^*}\right)$$

$$P^* = \frac{wh^3\Delta P}{12\eta LQ},\ V^{*+} = \frac{whv}{Q},\ T^{*+} = \frac{wh^2|\tau_y|}{6\eta Q},\ L^* == \frac{L_p}{L} \tag{11}$$

$$\Delta P = \begin{cases} a_1 P^* Q & 2L_p|\tau_y| < a_2 h|Q| \\ a_2 Q & 2L_p|\tau_y| \geq a_2 h|Q| \end{cases} \tag{12}$$

3. Magnetic Analysis and Design Parameters

Before determining the principal design parameters to meet the prespecified targets, the magnetic field distribution of the rotary MR damper needs to be undertaken. In this work, through the finite element analysis (FEA) simulations, the design elements are analyzed in terms of the rotational damping relative to input current. Additionally, computational fluid dynamics (CFD) analysis is performed to investigate sudden contraction phenomena during operation. The simulation is conducted using Ansys Fluent and Maxwell software (Ansys Company, Pennsylvania, USA, Ansys 14.5 Fluent, Ansys Maxwell 2018). Table 1 presents the specified parameters and other design parameters chosen from the solutions of the governing equations. These values are used to analyze the magnetic field distribution. The MR fluid, (MRF-132CG, Parker Lord, Cary, North Carolina, USA), is used as the representative nonlinear material, and its nonlinear data for the B-H curve are inputted as engineering data. The coil is made of AWG (American wire gauge) 21 wire with a diameter of 0.75 mm, and the applied current is set at 3A. The core material is specified as 1008 steel, a ferromagnetic material. The rotational speed is set to 30 m/s. The simulation results of the magnetic field are presented in Figure 6a. Now, based on the magnetic analysis result, the damping forces of the proposed rotary MR damper are calculated at various currents as a function of the rotational speed. Figure 6b shows the simulation results for the magnetic analysis i.e., the relationship between the field intensity and current, and also between the yield stress and current. As the magnetic field strength increases, the yielding stress becomes more pronounced. It can be observed that the magnetic field of approximately 200 kA/m is formed at the pole when the current of 3A is applied. Consequently, the yielding stress is approximately 40 kPa. This value is corroborated by the red line in Figure 7b.

Preprints.org (www.preprints.org) | NOT PEER-REVIEWED | Posted: 19 March 2024 doi:10.20944/preprints202403.1103.v1

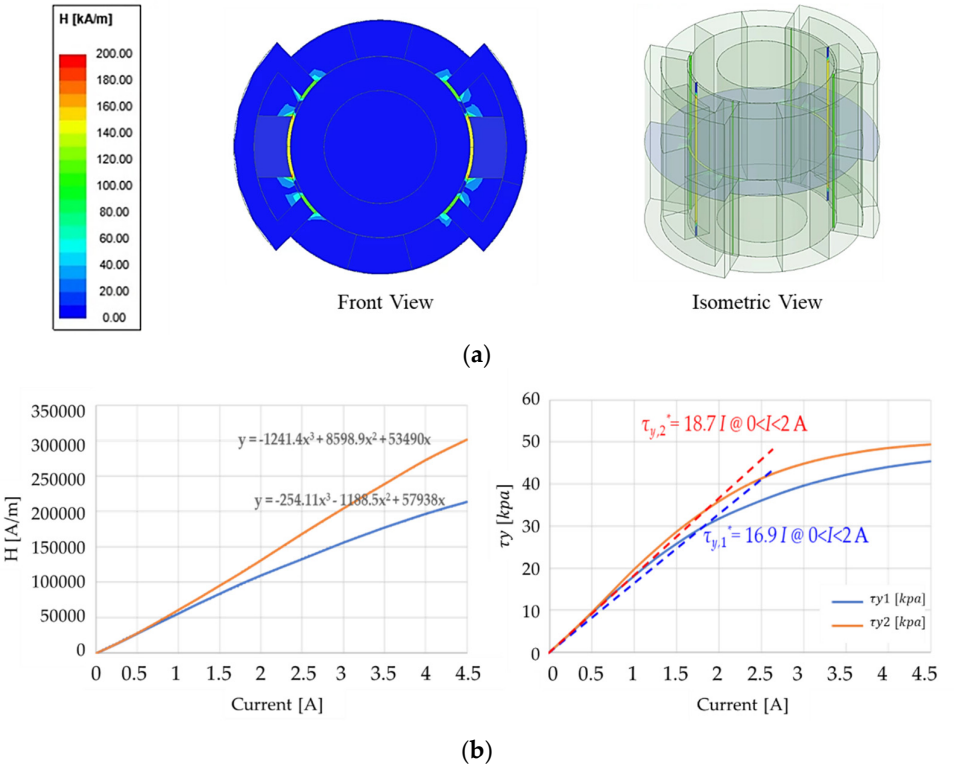

Figure 6. Magnetic analysis of the rotary MR damper; (a) contour view-front, isometric, (b) analysis results-between the yield stress and current.

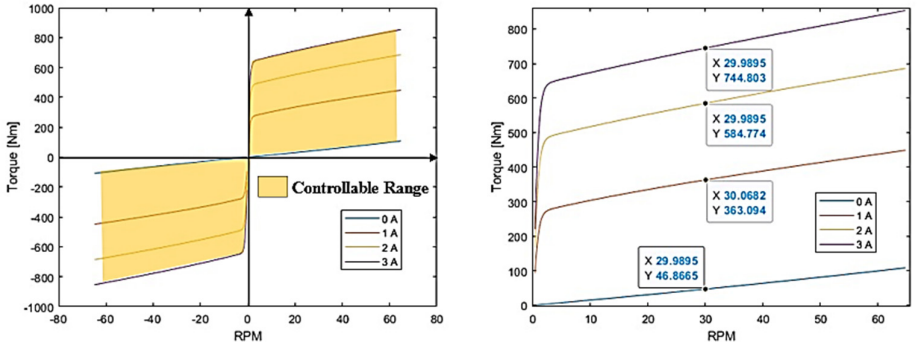

Figure 7. Simulation of the field-dependent torque of the rotary MR damper.

Table 1. Design parameter of the proposed rotary MR damper for the magnetic analysis.

Parameter name	Notation	Value
Max. Diameter	D	150mm
Max. Width	W	190mm
Vane Diameter	D_1 or D_v	125mm
Rotor Diameter	D_2 or D_r	79.1mm
Orifice width	w	82mm
Shaft Diameter	D_{shaft}	50mm
Shaft Length	L_{shaft}	294mm
Orifice Circumference Diameter	D_0	80.2mm

 doi:10.20944/preprints202403.1103.v1

Orifice Length	L_0 *or* L	63mm
Effective Pole Length	L_p	45mm
Orifice Gap Size	h	1.1mm

For the characterization and performance analysis of the proposed rotary MR damper, torque simulations are conducted at various current inputs and velocity levels. Figure 7 shows the simulation results showing the field-dependent damping torque. Through the simulations, the torque controllable range within the current range of 0 to 3A and M/S range of -60 to 60 are fixed as depicted in the left graph. The simulation results exhibited a symmetrical pattern around the origin. Calculations based on positive rpm values indicate torque values of 46.87Nm at 0A, 363.10Nm at 1A, 584.77Nm at 2A, and 744.80Nm at 3A, respectively. These values are proportional to the magnetic field. More specific results are summarized as follows. The fluid viscous rotational force (proportional to the rotational speed): 46.87Nm, Shear rotational force (proportional to the magnetic field): 697.9Nm (3A input), Total rotational force (viscous + shear rotational force).: 744.8 Nm (3A input), Outer diameter: 150 mm, Width (excluding shaft): 190 mm, Rotational angle capabilities: ±30° (Capable of rotating a total of 60 degrees) and MR fluid injection volume: 250ml.

As mentioned in Introduction, CFD analysis is also carried out in this work to analyze more accurate pressure drop of the proposed rotary MR damper. It is noted that In a system or device, the pressure imbalance may occur due to internal rotation or flow of the device. This phenomenon occurs when fluid flows rapidly or solid components move, leading to a rise in pressure. Such occurrences can impact the stability of the system and the durability of its components. As the designed damper experiences real-time changes in internal pressure, it is necessary to examine pressure drop profiles and velocity profiles. Furthermore, comparing pressure drops obtained from mathematical models and CFD simulations helps for the determination. The analysis conditions and simulation results are depicted in Figure 8. The analysis conditions are imposed as follows: The analysis is conducted under laminar flow conditions, with an input current of 0A, a flow velocity of 0.26m/s, and an angular velocity of 60rpm. The mathematical model yields a total pressure drop of 2.65 bar. The analysis indicates that the pressure drop is relatively low. In contrast, the CFD analysis affects to the total pressure drop of 4.04 bar. A comparison of the two values revealed a difference of approximately 1.4 bar. It was concluded that the difference, which is evaluated by 2%, could be considered negligible in design of the first prototype between two different analysis approaches. In the comparison between two results, there a little discrepancy in the rotational damping between the mathematical model and CFD analysis results, especially, when the current is not applied (off-state). However, the error in rotational damping is deemed negligible compared to the control range between current application (on state) and non-application (off state). Other factors contributing to this deviation may include frictional forces and temperature effects those are not considered in this work.

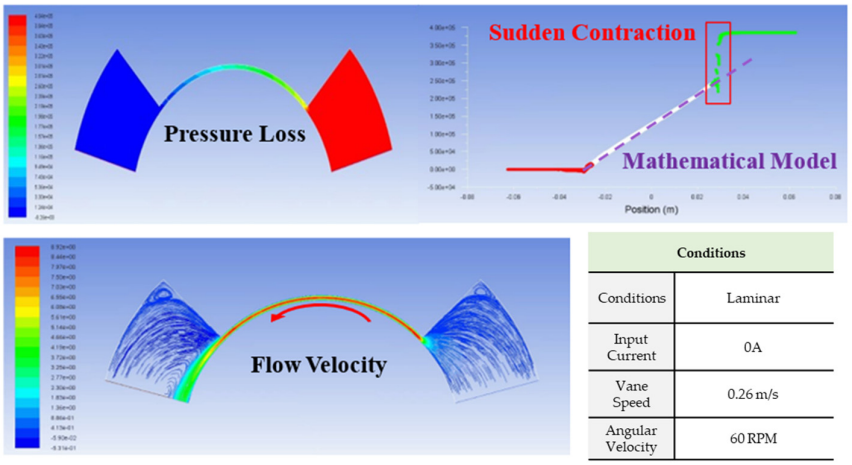

Conditions	
Conditions	Laminar
Input Current	0A
Vane Speed	0.26 m/s
Angular Velocity	60 RPM

 doi:10.20944/preprints202403.1103.v1

Figure 8. Pressure analysis of the rotary MR damper using CFD.

4. Experimental Results and Discussions

A prototype of the proposed rotary MR damper is manufactured as shown in Figure 9. This prototype is a semi-active damper and applicable to the vehicle suspension systems which have a low-floor level of a small-sized future cars. In Figure 10a, the final assembly covered with an external housing is shown. Assembled within are the shafts that can be connected and attached to the vehicle's axle or suspension. Figure 8b displays the internal core filled with MR fluid. Figure 10 presents an experimental setup for measuring damping force of the rotary MR damper under the sinusoidal excitations. The damping force is measured by the load cell, while the displacement of the excitation and stroke is measured by the transducer wire sensor. In addition, the servo hydraulic system exciters the damper, the current amplifier and data acquisition system are also used. The experiment is conducted in the consistent environment with a displacement of ±30 mm (rotation ≅30°), an excitation frequency of 1 Hz, and a maximum of 15 rpm (0.2m/s). As seen from the experimental apparatus, the hydraulic exciter originally produces the dynamic motions in the vertical direction only. However, in this test, the vertical motion is converted to the rotational motion using the jigs and fixtures. In order to investigate the effect of the exciting directions from the linear to rotation to the discrepancy, each test is carried out more than 5 times and the average values used for the presentation of the results. It is noted here that the legend of MR damper stands for the rotary MR damper to be tested with the rotational motion.

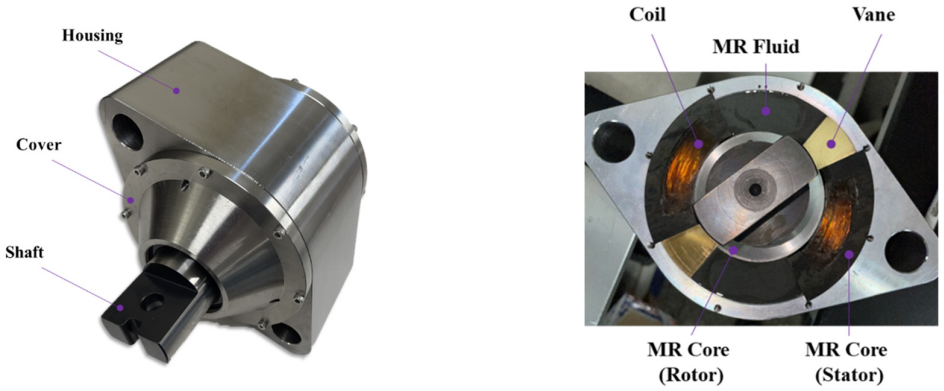

Figure 9. The prototype of the proposed rotary MR damper; (a) assembled, (b) magnetic circuit core.

 doi:10.20944/preprints202403.1103.v1

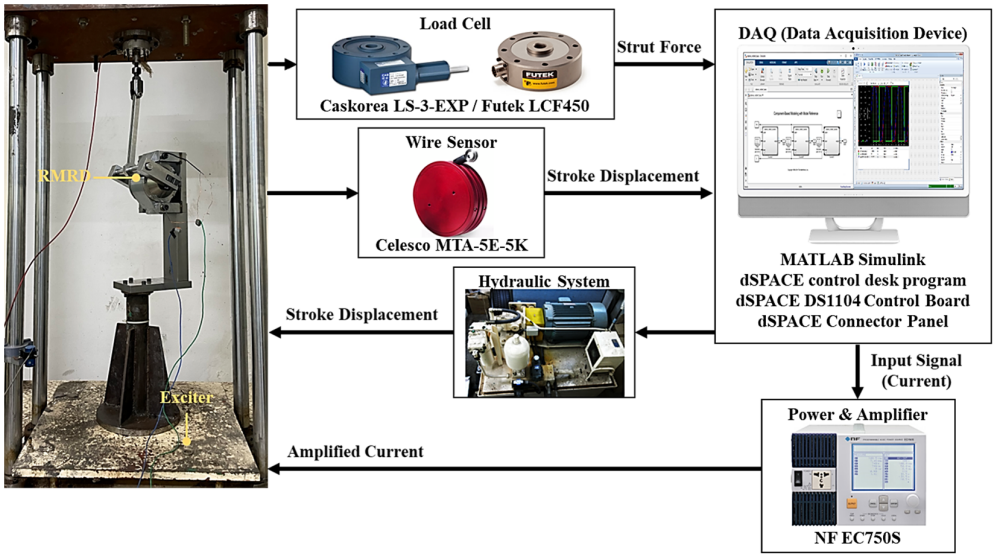

Figure 10. Experimental apparatus for the damping force measurement.

4.1. Damping Force

Figure 11 shows the field-dependent force achieved from the first test. It is tested in the same way as the linear MR damper by exciting continuously changing the frequency and magnitude. It is clearly seen that there exist severe noises which may affect the damping force. Moreover, it is found that there is problem in the motion converter. As a result, a large error occurred when compared to the simulation value, so the experimental analysis is conducted immediately. It is determined that the cause of the error is occurred in the part where the core inside the damper and the rotor to be contacted produces rolling friction that occurs as the rotor rotates. It is also discovered that when the magnetic field is formed in this area and holds the rotor, and then the fluid detours between the contact between the rotor and the core. Due to this phenomenon, the fluid does not accumulate in the designed orifice, but it flows to an unexpected place, resulting in a lower damping force than expected. It should be noted here that a rotary type of test equipment integrating with the torque sensor and encoder needs to be used to achieve more accurate damping force, angular velocity. However, due to the lack of such a test equipment, in this work the low pass filter and lubrication oils are used during the test to compensate the noise and friction effects. The tolerance occurred in the motion converter is also reduced before testing again. Figure 12 shows the results after modifying the experimental apparatus. It is noted that in this test, the discrete result at a certain velocity (or rpm) is acquired to make the result point more clearly. The points in the measured results are the tested m/s. Figure 12a presents the simulated force-velocity (F-V) graph, showing hysteresis curves formed in both extension and compression directions for each current. It is found that the force increases or decreases proportionally to the velocity by approximately 1kN per turn within the velocity range of -0.2m/s to +0.2m/s. Thus, it can be inferred that damping force proportional to velocity occurs for input currents beyond a certain level within block up region. The measure damping force is shown in Figure 12b achieved from the same operating conditions except the data acquisition method where the discrete damping force is collected at a certain one m/s condition. It is identified from two results that the maximum damping force achieved from experiment is little less than the simulated result at the same piston velocity. It should be noted here that the maximum force shown in Figure 12b at 0.2 m/s is almost equivalent to the desired damping torque of 600 Nm.

 doi:10.20944/preprints202403.1103.v1

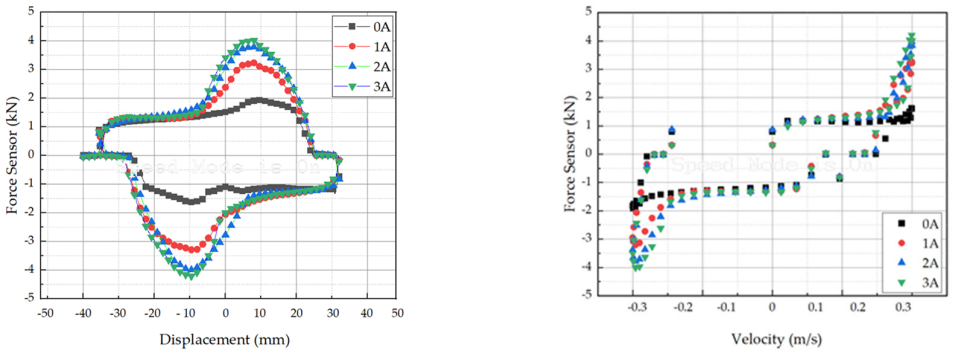

Figure 11. Damping force experiment result data with simulation data reapplied with the 0.2m/s 0 ~ 3A: (a) F-D curve for 0.2m/s, (b) F-V curve for 0.2m/s.

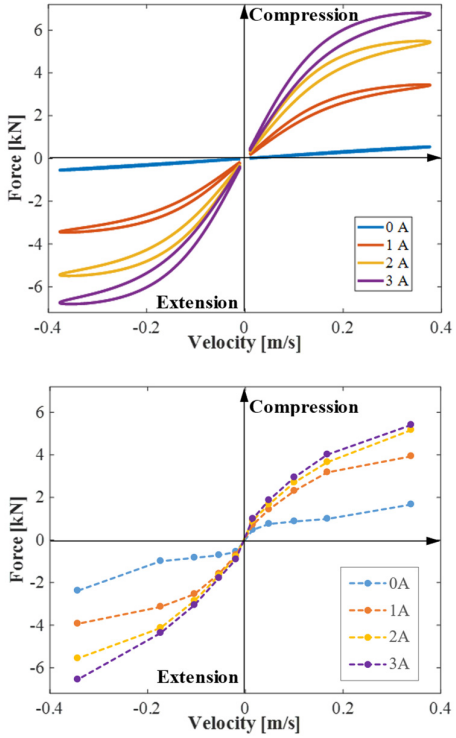

Figure 12. Damping characteristics in F-V curve; (a) simulation, (b) measurement.

4.2. Response Time Measurement

One of salient properties of MR fluid is the fast reversible response time which can be adaptable to various dynamic systems subjected to relatively high frequency disturbances. As a vehicle suspension system, there are two significant vibration modes: 1st mode (car body mode) and 2nd mode (wheel mode). In order to cover both modes, the response time of the suspension system should be faster than 50 ms at least. Therefore, the response time of MR damper itself needs to be faster than 30 ms to avoid the adverse effect from the time delay. In general, in order to achieve the fast response time of MR damper, several methods have been carried out. For examples, the use of the register in the magnetic circuit, the reduction of the eddy current, surface groove of the magnetic pole and others. In this work, a simple PI control circuit is used to achieve fast response time of the rotary MR damper. Figure 13 shows the configuration of the current control PI controller integrated with the MR damper in which PI controller can help improve the response time of overall control looping time. Table 2

 doi:10.20944/preprints202403.1103.v1

shows the measurement results of the response time of the proposed MR damper with the PI circuit shown in Figure 13. Since the inductance increases as the current increases and hence the impedance is expected to decrease. This reaction speed is expected to improve when a high current is applied. When constant voltage is applied instead of the PI controlled voltage, there is a very little difference in rising time within 10ms. It is also observed from the results that the rise time becomes longer when the 60 Ohm register is added to the PI circuit. The finding of the solution to resolve this problem takes a time and hence it is not treated in this work. However, it is surely found that the rise time in most of cases is less than 50 MS which is the target value. Therefore, the prototype rotary MR damper which is applicable to the low-body floor vehicle suspension system or PBV suspension system can be a novel candidate for the suspension system of special vehicles to be appeared in UMC.

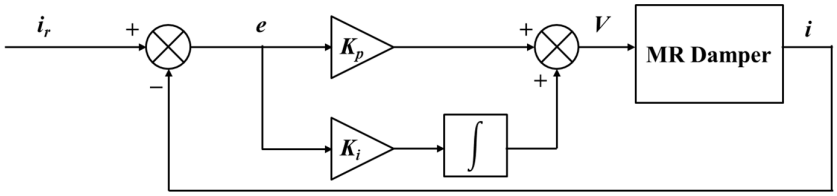

Figure 13. PI control block-diagram to achieve fast response time of the rotary MR damper.

Table 2. Measured response time of the rotary MR damper evaluated at 90% of the rise time.

Type	K_p	K_i	Rise Time (Up, cycles)	Rise Time (ms)	Remark
0A → 3A	2	10	12	22ms	
	2.5	10	11	20ms	
	3.5	10	11	20ms	
	1	10	16	30ms	
	0.5	10	18	34ms	
	0.5	5	20	38ms	
	2.5	5	14	26ms	
	2.5	1	13	24ms	
	2.5	15	13	24ms	
	4.0	10	16	30ms	
	2.5	0	14	26ms	
	5	0	14	26ms	
0A → 1A 60 Ohm added	2.5	10	469	936ms	Problems expected during control
	5	10	416	830ms	
0A → 1A	2.5	10	79	156ms	Abnormal behavior expected
	5	0	82	162ms	

5. Conclusion

In this study, a new type of the rotary MR damper applicable to the low-body floor vehicle suspension system was designed and its effectiveness was demonstrated through the testing of the prototype. In the design process, the targets of the design parameters and maximum damping force were firstly specified unlike other research works. After formulating the governing equations of morion in non-dimensional domain, the pressure drop and flow motion were analyzed, followed by the magnetic field analysis through both the finite element method and CFD approach. Therefore, principal design parameters to achieve the prescribed targets have been determined and the field-dependent damping force are achieved in the force versus velocity (rotational speed). After validating from the simulation results that the target specifications could be obtained using the determined

 doi:10.20944/preprints202403.1103.v1

design parameters, a prototype of the rotary MR damper was manufactured and tested. It was confirmed that the target maximum damping force of 600 Nm could be achieved from the prototype and the target rise response time of 50 ms also could be easily obtained by integrating a simple PI electric circuit. It is finally noted as future works that some benefits to be expected from the proposed rotary MR damper should be deeply explored more focusing on compact size, small amount of MR fluid, less sealing problem, low energy consumption, less particle settling problem due to the rotation motion, higher damping force through the optimization and longer durability for practical feasibility.

Author Contributions: Conceptualization, B-H.K, S.-B,C ; methodology, B.-H,K; software, B.-H,K; mathematical modeling, B.-H,K, validation, B.-H,K, U ; formal analysis, B.-H,K; investigation, B.-H,K; data curation, B.-H,K; writing—original draft preparation, Y-.J,P.; writing—review and editing, S.-B,C; visualization, B-.H,K, Y-J,P.; supervision, S.-B,C.; project administration, S.-B,C.; All authors have read and agreed to the published version of the manuscript.

Funding: There is no funding for this research.

Data Availability Statement: Available upon the request from the potential readers.

References

1. https://www.bwigroup.com/solutions/
2. https://www.shoplordmr.com/products
3. Lee, Jong-Woo, Min-Sang Seong, Je-Kwan Woo, and Seung-Bok Choi. "Modeling and Vibration Control of Small-Sized Magneto-Rheological Damper." Transactions of the Korean Society for Noise and Vibration Engineering 22, no. 11 (2012): 1121-27.
4. Bai, Xian-Xu, Wei Hu, and Norman M Wereley. "Magnetorheological Damper Utilizing an Inner Bypass for Ground Vehicle Suspensions." IEEE Transactions on Magnetics 49, no. 7 (2013): 3422-25.
5. Weber, F. "Semi-Active Vibration Absorber Based on Real-Time Controlled MR Damper." Mechanical Systems and Signal Processing 46, no. 2 (2014): 272-88.
6. Sohn, Jung Woo, Jong-Seok Oh, and Seung-Bok Choi. "Design and Novel Type of a Magnetorheological Damper Featuring Piston Bypass Hole." Smart Materials and Structures 24, no. 3 (2015): 035013.
7. Giorgetti, Alessandro, Niccolo' Baldanzini, M Biasiotto, and Paolo Citti. "Design and Testing of a MRF Rotational Damper for Vehicle Applications." Smart Materials and Structures 19, no. 6 (2010): 065006.
8. Lee, Jae-Hoon, Changwan Han, Dongsu Ahn, Jin Kyoo Lee, Sang-Hu Park, and Seonghun Park. "Design and Performance Evaluation of a Rotary Magnetorheological Damper for Unmanned Vehicle Suspension Systems." The Scientific World Journal 2013 (2013).
9. Imaduddin, Fitrian, Saiful Amri Mazlan, and Hairi Zamzuri. "A Design and Modelling Review of Rotary Magnetorheological Damper." Materials & Design 51 (2013): 575-91.
10. Imaduddin, Fitrian, Saiful Amri Mazlan, Hairi Zamzuri, and Mohd Azizi Abdul Rahman. "Bypass Rotary Magnetorheological Damper for Automotive Applications." Applied Mechanics and Materials 663 (2014): 685-89.
11. Sapiński, Bogdan. "Experimental Investigation of an Energy Harvesting Rotary Generator-MRF Damper System." Journal of Theoretical and Applied Mechanics 54, no. 3 (2016): 679-90.
12. Yu, Jianqiang, Xiaomin Dong, Xi Su, and Song Qi. "Development and Characterization of a Novel Rotary Magnetorheological Fluid Damper with Variable Damping and Stiffness." Mechanical Systems and Signal Processing 165 (2022): 108320.
13. Kumbhar, Bhau K, Satyajit R Patil, and Suresh M Sawant. "Synthesis and Characterization of Magneto-Rheological (MRF) Fluids for Mr Brake Application." Engineering Science and Technology, an International Journal 18, no. 3 (2015): 432-38.
14. Latha, K Hema, P Usha Sri, and N Seetharamaiah. "Design and Manufacturing Aspects of Magneto-Rheological Fluid (MRF) Clutch." Materials Today: Proceedings 4, no. 2 (2017): 1525-34.
15. Zhang, Huan, Haiping Du, Shuaishuai Sun, Weihua Li, and Yafei Wang. Design and Analysis of a Novel Magnetorheological Fluid Dual Clutch for Electric Vehicle Transmission. SAE Technical Paper (2019).
16. East, William, Jérôme Turcotte, Jean-Sébastien Plante, and Guifré Julio. "Experimental Assessment of a Linear Actuator Driven by Magnetorheological Clutches for Automotive Active Suspensions." Journal of intelligent material systems and structures 32, no. 9 (2021): 955-70.
17. Wang, Daoming, Guangxin Yang, Yangjun Luo, Shirui Fang, and Tao Dong. "Optimal Design and Stability Control of an Automotive Magnetorheological Brake Considering the Temperature Effect." Smart Materials and Structures 32, no. 2 (2023): 025020.
18. http://www.ces.tech.

 doi:10.20944/preprints202403.1103.v1

19. Billie Jr, FS. "" Smart" Dampers for Seismic Protection of Structures: A Full-Scale Study." Paper presented at the Proc. Second World Conference on Structural Control, Kyoto, Japan, June 28-July 1, 1998, 1998.
20. Khan, Md Sadak Ali, A Suresh, and N Seetha Ramaiah. "Analysis of Magnetorheological Fluid Damper with Various Piston Profiles." International Journal of Engineering and Advanced Technology 2, no. 2 (2012): 77-83.
21. Kang, Byung-Hyuk, Jai-Hyuk Hwang, and Seung-Bok Choi. "A New Design Model of an MR Shock Absorber for Aircraft Landing Gear Systems Considering Major and Minor Pressure Losses: Experimental Validation." Applied Sciences 11, no. 17 (2021): 7895.